Journal of Advances in Manufacturing Engineering
Web page info: https://jame.yildiz.edu.tr
DOI: 10.14744/ytu.jame.2024.00009

Original Article

Dry sliding wear behaviour of Ti13Nb13Zr alloy produced via pressure-assisted sintering

Mustafa ARMAĞAN*

Department of Mechanical Engineering, İstanbul Medeniyet University, İstanbul, Türkiye

ARTICLE INFO

Article history
Received: 11 November 2024
Revised: 27 November 2024
Accepted: 01 December 2024

Key words:
Friction, titanium alloys, tribology, sintering, surface morphology.

ABSTRACT

Novel alloys and advanced manufacturing methods may improve titanium-based materials' mechanical, corrosion, and biocompatibility properties. Specifically, the Ti13Nb13Zr alloy has recently garnered significant attention for orthopaedic applications, where adequate wear resistance is essential. The present paper aims to reveal dry sliding wear behaviour of the Ti13Nb13Zr alloy produced via pressure-assisted sintering. Ti13Nb13Zr samples were tested under different loads (10, 15, and 20 N) in a ball-on-disc dry sliding test system. The coefficient of friction (CoF) curves obtained to demonstrate dry sliding wear behaviour of the alloy, and the worn surface morphologies were examined to understand the underlying wear mechanisms. The mean coefficient of friction (CoF) values (and standard deviations) for the specimens subjected to increasing loads were 0.445 (0.0182), 0.480 (0.0205), and 0.465 (0.0167), respectively. Furthermore, the specific wear rates after wear were also found to be $3.76x10^{-3}$, $4.24x10^{-3}$, and $4.5x10^{-3}$ in the same order. Histogram analyses and weight loss values indicate that the 20 N test load exhibited the highest wear rate. The surface morphology was characterised by scanning electron microscopy, and energy dispersive X-ray spectroscopy (EDS) investigations were conducted. The formation of grooves and scratches was attributed to abrasive wear. The occurrence of wear debris at loads of 15 and 20 N resulted in the development of a three-body wear mechanism. Moreover, elemental mapping analysis demonstrated that the transfer of alumina ball particles on the worn surface at higher loads.

Cite this article as: Armağan, M. (2024). Dry sliding wear behaviour of Ti13Nb13Zr alloy produced via pressure-assisted sintering. *J Adv Manuf Eng*, 5(2), 00–00.

INTRODUCTION

Titanium and its alloys are frequently preferred in the aerospace and biomedical industries due to their superior mechanical, corrosion, and biocompatibility properties. However, the ever-increasing high-efficiency performance requirements of industries and end-users have prompted researchers to explore the potential of new titanium alloys [1–6]. The innovative Ti13Nb13Zr titanium alloy has recently attracted considerable interest from the research community [7]. The strong β-phase effect of Nb and Zr gives the titanium alloy enhanced performance and machinability [8]. Furthermore, the release of toxic elements in Ti6Al4V and the stress-shielding effect of the conventional CpTi alloy can be eliminated by the composition of Ti13Nb13Zr [9].

In the relevant literature, the Ti13Nb13Zr titanium alloy is predominantly manufactured through conventional techniques, including casting and forging [10, 11]. Furthermore, researchers typically procure the alloy from commercial sources [12–14]. Additionally, recent studies have sought to employ a range of processing methodologies with the intention of enhancing the overall performance of the alloy

***Corresponding author.**
*E-mail address: mustafaarmagan@hotmail.com.tr

[8, 15–21]. The Ti13Nb13Zr alloy is of considerable interest for orthopaedic applications [16, 22–25], making the understanding of its tribological properties and behaviour a critical concern. Thus, the Ti13Nb13Zr alloy has recently garnered significant attention for orthopaedic applications, where adequate wear resistance is essential [1, 21, 26–29]. Piotrowska et al. [30] investigated the tribological properties of the Ti13Nb13Zr alloy by coating it with a diamond-like carbon coating via the physical vapour deposition method. The coating resulted in a notable reduction in the coefficient of friction in all three tested media, namely dry friction, synovial fluid, and Ringer's solution. Neto and Rainforth [11] conducted an investigation into the wear behaviour and mechanisms [31] of the alloys produced by arc melting as a result of tribocorrosion tests. Piotrowska and Madej [32] observed a reduction in wear and an increase in hardness when a TiO_2 coating was applied to the alloy surface using the atomic layer deposition technique. Piotrowska et al. [33] modified the tribological properties of the alloy by altering the surface roughness prior to deposition of an a-C:H:Si coating via plasma-assisted chemical vapour deposition. In a study conducted by Seramak et al. [34], the porosity, microstructure, and compressive strength of samples produced by sintering powders with varying grain sizes were characterised. Results suggested these samples could be used in load-bearing implants.

Recent literature suggests that Ti13Nb13Zr alloy produced via powder metallurgy have an interesting field of research, while further research is required to elucidate their tribological behaviour. The present paper aims to reveal dry sliding wear behaviour of Ti13Nb13Zr alloy produced via pressure-assisted sintering. Ti13Nb13Zr samples were tested under different loads (10, 15, and 20 N) in a ball-on-disc dry sliding test system. The coefficient of friction along the sliding distance were determined. By analysing the histogram graphs and mass loss values together, the wear behaviour for the applied loads was described. Finally, the wear morphologies were discussed by electron microscopy, and the interactions between the alloy and the counterface (Al_2O_3 ball) were investigated by energy dispersive X-ray spectroscopy (EDS) and elemental mapping.

Table 1. Wear test parameters

Parameter	Values	Units
Disc rotation speed	150	rpm
Trace diameter	12	mm
Velocity	94.24	mm/sec
Time	2653	sec
Distance	250000	mm
Nominal force	10, 15, 20	N
Temparature	25	°C

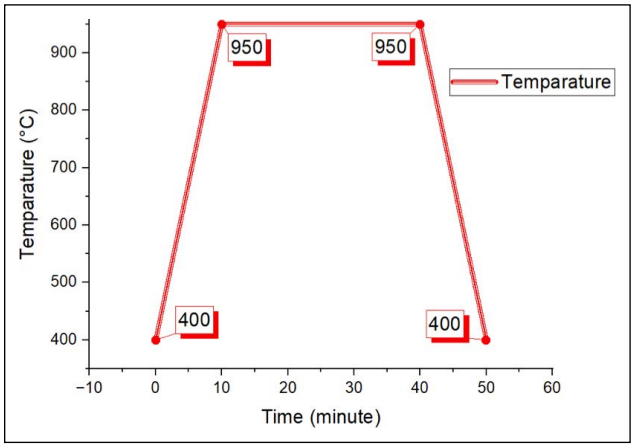

Figure 1. Sintering production cycle.

MATERIALS AND METHODS

Production of Ti13Nb13Zr Samples

To manufacture the Ti13Nb13Zr alloy via powder metallurgy, powders comprising Ti, Nb, and Zr were obtained from Nanography Nano Technology (Türkiye), a commercial supplier of these materials. The uniformly mixed powders were subsequently positioned in graphite moulds measuring 20 mm in diameter and 4 mm in height. To mitigate potential inconsistencies arising from the mould design and fabrication, graphite paper was applied between the mould and the powder. The mould punches were set

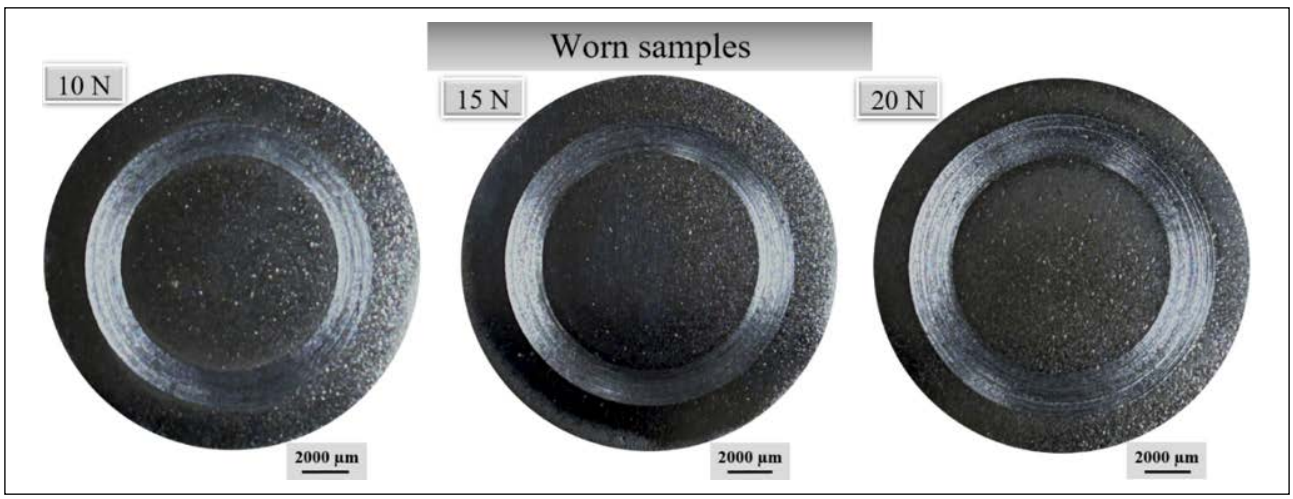

Figure 2. Macro images of the worn samples.

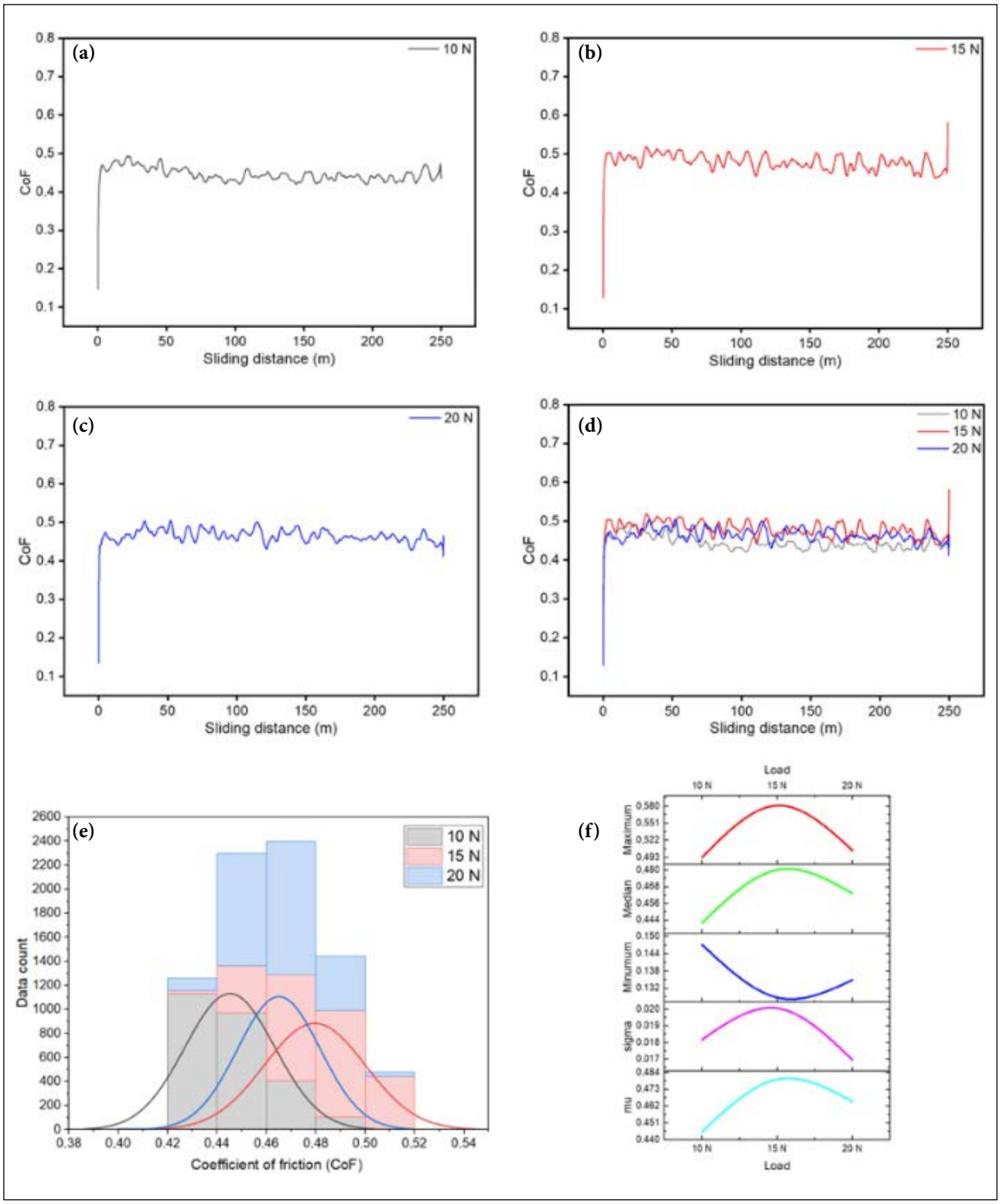

Figure 3. CoF values versus sliding distance **(a)** 10 N, **(b)** 15 N, **(c)** 20 N, **(d)** overlapping curves; statistical CoF values **(e)** histogram, **(f)** maximum, median, minimum, sigma and mu values.

up to an equivalent height to ensure a consistent temperature gradient during the sintering process. The moulds were prepared for production and exposed to a vacuum of 10^{-4} mbar and a pressure of 14 kN in a hot press apparatus produced by the DIEX brand (China). Consequently, oxidation was inhibited through the application of vacuum, and denser samples were generated by exerting pressure. The samples were acquired following a production cycle with a total sintering duration of 50 minutes and a temperature range of 400 °C to 950 °C (Fig. 1). The sintered samples were permitted to cool in the hot press for 10 minutes before being cooled to room temperature.

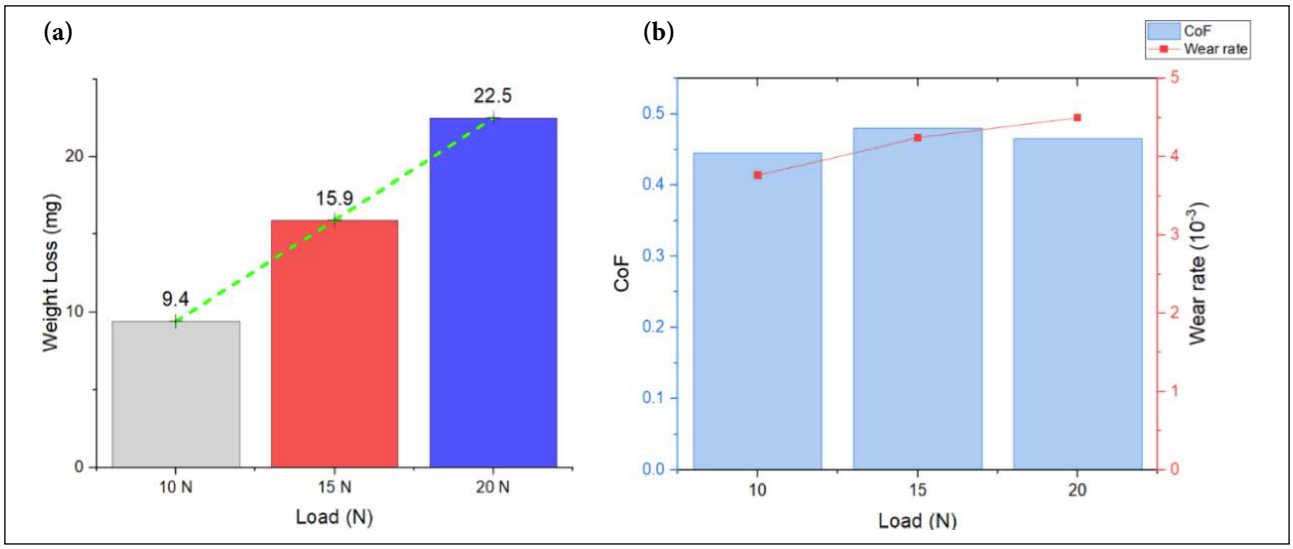

Figure 4. **(a)** Weight loss versus loads; **(b)** CoF and wear rate versus loads.

Tribological Testing

Before tribological testing, the sintered samples received metallographic procedures. To accomplish this, the samples were subjected to grinding with abrasives ranging from 320 to 1000 grit (utilising a force of 40N and a rotational speed of 300 rpm) and subsequently polished with diamond solutions of 9 µm, 3 µm, and 1 µm, respectively (applying forces of 30N, 20N, and 15N in accordance with the diamond size, at a rotational speed of 300 rpm).

Tribological tests were conducted on samples using a ball-on-disc tribometer (Turkyus brand, Türkiye). Al_2O_3 balls with a diameter of 6 mm were utilised as the counter surface for the wear tests. The parameters utilised in the wear tests are detailed in Table 1, and the macro images of the specimens are displayed in Figure 2. The coefficient of friction (CoF) was documented and examined by the tester during the test. Additionally, the weights of the samples were quantified using a precision balance prior to and following the wear test, and the weight losses were computed. Based on these measurements, specific wear rates were then calculated. A specific wear rate (usually specific wear or wear rate) that is the volume (or sometimes the mass) loss per unit force per unit distance of a body in motion against another one. The calculation of specific wear (k) rate is seen in Eq. (1).

$$k = \frac{m}{W\ x\ L}$$

Where m is weight loss (mg), W is applied load (N), and L is sliding distance (m).

Subsequently, worn surface morphologies of the samples were investigated using a Thermo Scientific Quattro S brand (Germany) environmental scanning electron microscope (ESEM) to ascertain the wear mechanisms following the wear test. Additionally, energy dispersive X-ray spectroscopy and elemental mapping were employed on the wear zone to identify the formation of wear debris and oxidation of the surface during dry sliding contact.

RESULTS AND DISCUSSION

Variation of Coefficient of Friction and Weight Loss

One of the key indicators that elucidates the dry sliding wear behaviour of the Ti13Nb13Zr alloy is the coefficient of friction (CoF) value. To this end, the CoF curves over a sliding distance of 250 m for loads of 10, 15, and 20 N are presented in Figures 3a–c. The tendencies of the curves for all three load parameters were comparable rendering them unable to illustrate the differences in tribological behaviour with various loads (Fig. 3d). However, it is anticipated that each applied test load will exhibit a distinctive wear mechanism on the alloy surface. Thus, Figures 3e and f characterise the effects of load variations on CoF values by means of statistical analyses dealing with all test data. In the histogram plots, which are normally distributed (Fig. 3e), the peak regions of the same CoF values for all data are characterised by curve and column plots. The mean CoF values for the main peaks (0.445, 0.465, and 0.480) were determined for loads of 10, 20, and 15 N, respectively. However, the acceptance criterion for the average CoF due to the main peak can be accepted when the three curves show similar span. For loads of 10 and 20 N, a similar aperture was observed, but for 15 N, the curve aperture was greater. This indicated that the CoF values were distributed over a wider scale.

It is desirable that the dry sliding wear behaviour exhibits minimal deviation in the CoF value along the sliding distance. This approach yielded standard deviation values of 0.017, 0.018, and 0.020 for 20, 10, and 15 N, respectively. The 20 N load demonstrated superior wear resistance, exhibiting a CoF value that was proximate to the highest average value observed for the 15 N load and displaying the lowest standard deviation. Figure 3f illustrates the behaviour of the maximum, minimum, median, sigma (error), and mu (mean) values in response to variations in load parameters. When these values are evaluated collectively for each load parameter, the superior 20 N CoF result is evident.

Figure 4a illustrates the weight loss associated with dry sliding wear as a function of increasing load. A direct cor-

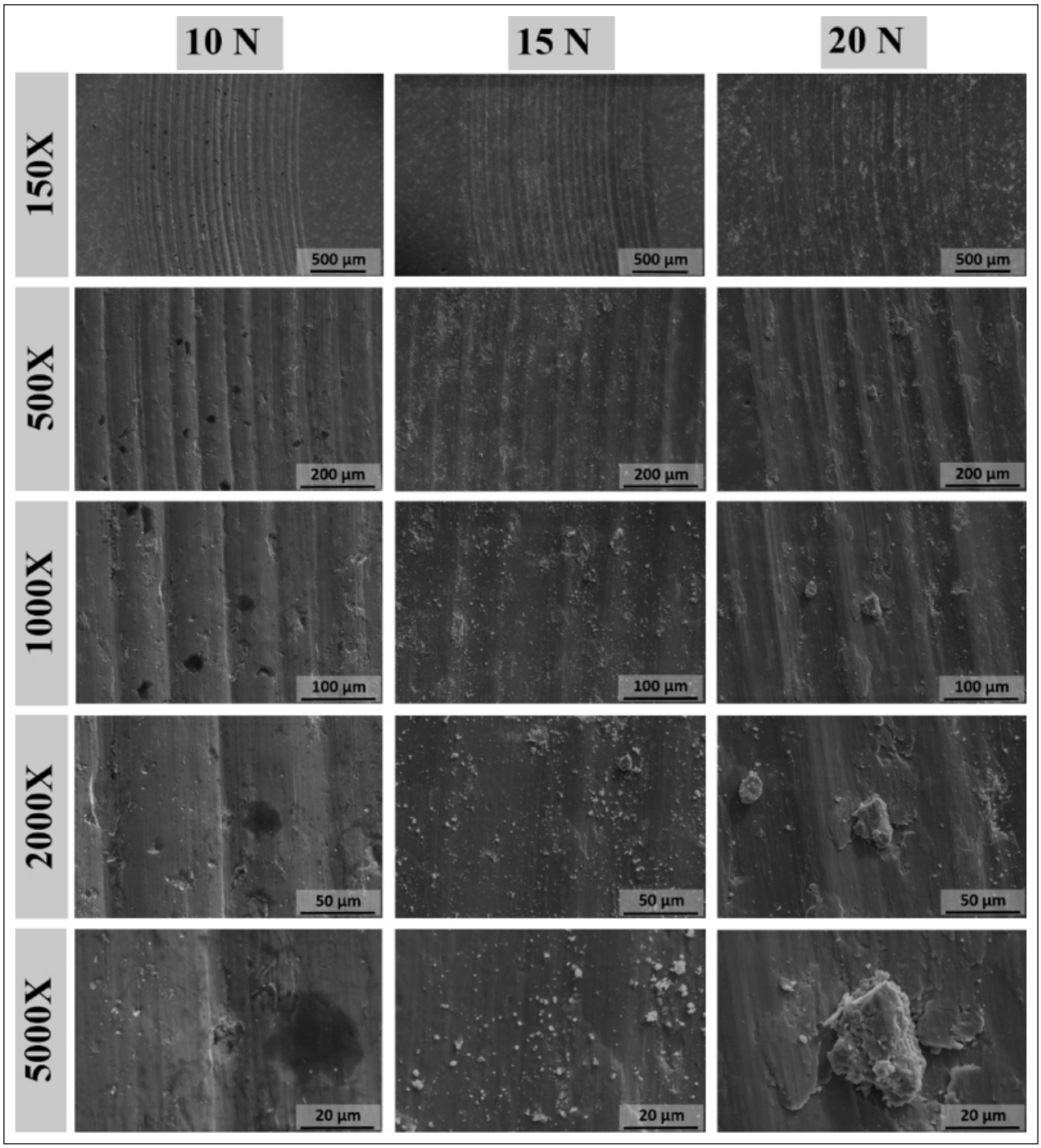

Figure 5. SEM images of worn surfaces under 10, 15, and 20 N load at magnification ratios between 150X-5000X.

relation was identified between the test load and the weight loss, with an observed increase of approximately 139.4%. Therefore, despite minor discrepancies in the mean CoF, a significant trend was observed in the weight loss as a function of load. The maximum weight loss was observed at a load of 20 N, which corroborates the statistical analysis result for the CoF coefficient. Furthermore, as indicated by Eq. 1, the specific wear rate values were determined to be $3.76x10^{-3}$, $4.24x10^{-3}$, and $4.5x10^{-3}$ for 10, 15, and 20 N, respectively (Fig. 4b). In dry sliding wear, the wear behaviour of materials is significantly affected by a number of factors, including the applied load, sliding distance, counter material, sliding speed, and so forth [35]. In this regard, the ball-on-disk principle in the literature employs a 250 m sliding distance [36–39], a 10-20 N load range [37–42], and an Al_2O_3 [42, 43] counter surface type. Consequently, the results obtained with these selection criteria were interpreted and supported. The values for CoF [44, 45], volume loss [41], wear rate [41, 44, 45], and specific wear rate [46] demonstrated an increase with the application of an increasing load. By integrating the evaluation of CoF, weight loss and wear rate results, a more precise inference about

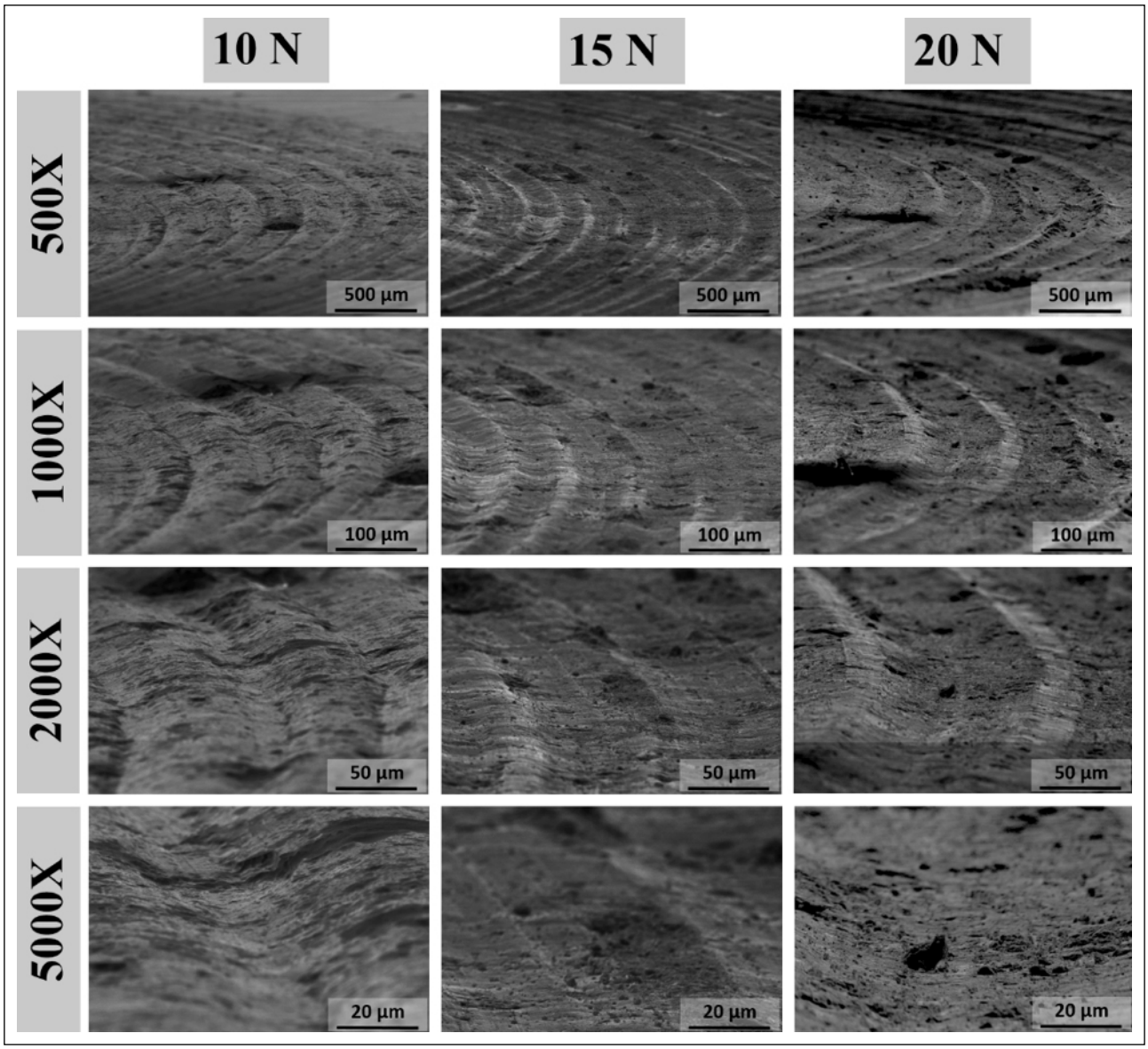

Figure 6. Tilt angle SEM images of wear grooves under 10, 15 and 20 N load at magnification ratios between 500X-5000X.

the wear resistance could be made. Additionally, the results will be discussed in the following section, taking into account the worn surface morphologies, and the dry sliding wear behaviour will be characterised in all aspects.

Worn Surface Morphology

Figure 5 depicts the surface morphologies of the Ti13Nb13Zr alloy after dry sliding tests conducted at loads of 10, 15, and 20 N. The cumulative sliding widths measured were 1609 µm, 1700 µm, and 1947 µm for applied forces of 10 N, 15 N, and 20 N, respectively. The observed increase in track width with increasing load was consistent with the CoF and weight loss results. The worn surface at 10N demonstrated significant material detachment; however, the absence of detached particles suggests that the two-body abrasive wear mechanism was the primary process. Moreover, abrasion wear led to the development of grooves and scratches [2, 42] in the friction zones, with a more significant accumulation of plastic deformation noted at the groove boundaries than in the tests performed at loads of 20 and 15 N. At loads of 15 and 20 N, the size of the grooves and scratches caused by abrasion on the surface increased with increasing load. Additionally, the material particles that were broken off increased in accordance with the load, forming a three-body wear mechanism [2, 6, 35].

Figure 6 presents a comparison of the surface morphologies, with the formation geometries of the wear channels determined through a tilt angle SEM view at five degrees to the wear axis. At a load of 10 N, the accumulation of excessive plastic deformation was observed in the wear channels [42]. Furthermore, the distance between the channels was observed to increase with increasing load, reaching approximately 73, 88, and 155 µm, respectively. At loads of 15 and 20 N, detached materials [2] were observed in the grooves, with an increase in the amount of material observed with increasing load. This supports the formation of a three-body wear mechanism [35] for both loads. Notably, the surface damage was particularly severe at 20 N, which aligns with the CoF and wear loss results.

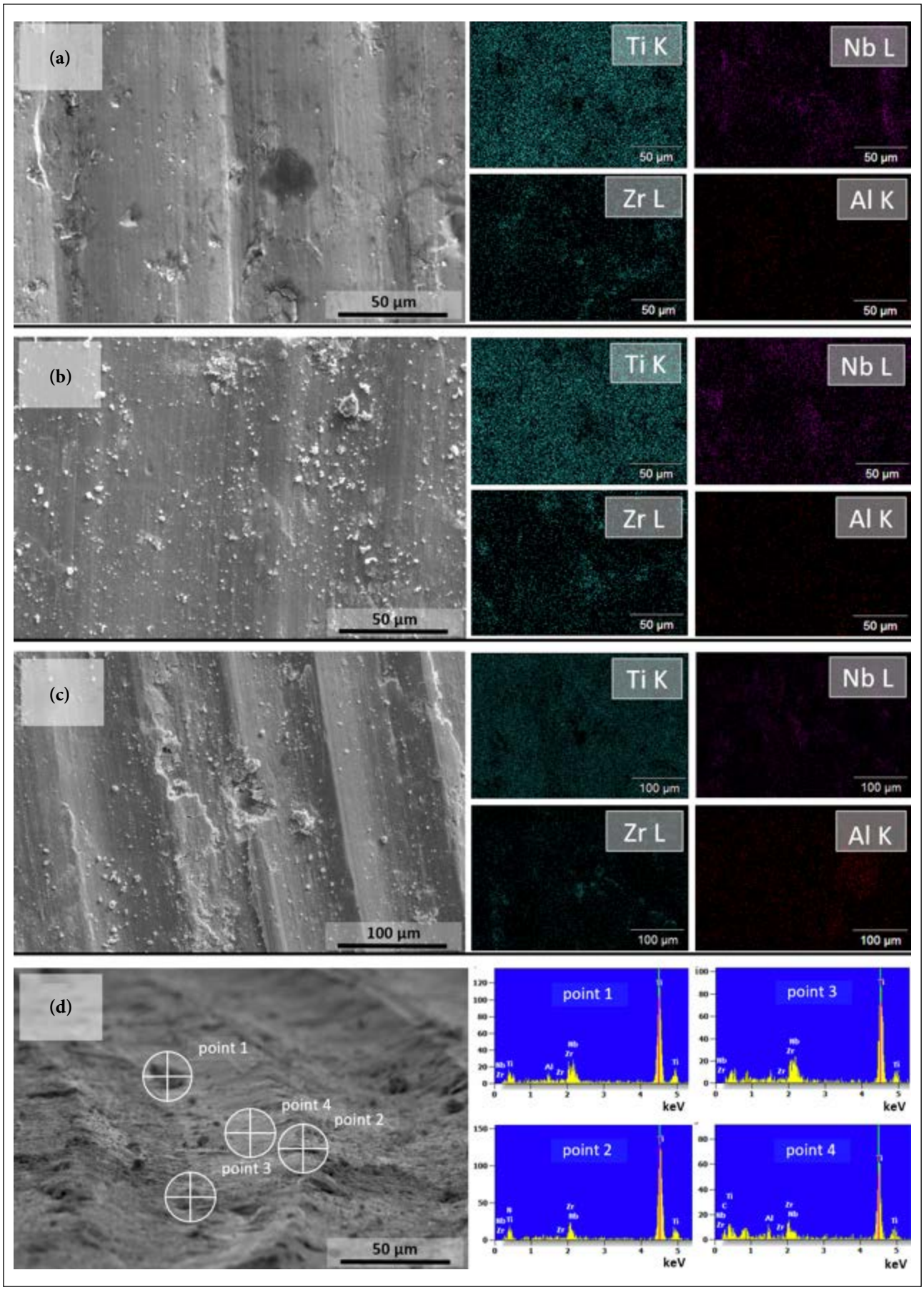

Figure 7. EDS and elemental mapping for sliding surfaces **(a)** 10 N, **(b)** 15 N, **(c)** 20 N; sliding surfaces at an angle of five degrees to the channel axis for EDS **(d)** 20 N.

Energy-dispersive spectroscopy (EDS) and elemental mapping are highly effective techniques for elucidating the formation of surface morphologies resulting from dry sliding, surface oxidation [2], the influence of the counter friction element [42], and the development of wear mechanisms [43]. Figures 7a–c illustrate the results of EDS and elemental mapping analyses conducted for loads of 10, 15, and 20 N, respectively. The presence of oxygen and aluminium in the point spectra of the fractured materials can be attributed to transfer from the alumina ball. The lack of oxygen distribution in the elemental mapping results excluded oxidation as a contributing factor to wear behaviour of the alloy. The elemental mapping analysis revealed that the percentage of Al element increased with increasing load, thereby corroborating the conclusion of the ball transfer effect [6, 41]. Figure 7d depicts the point EDS spectra obtained at an angle of five degrees to the channel axis under a 20 N load. The absence of oxygen in all point spectra and the presence of aluminium in some points substantiated the conclusion of no oxidation [2] and the transfer effect of the alumina ball [6, 41].

The production of the innovative Ti13Nb13Zr alloy by pressure-assisted sintering permitted the dry sliding behaviour to be characterised. The consistent and predictable behaviour of the CoF coefficients, with minimal deviation, and the morphological findings negated the necessity for surface treatments, such as surface coating, to achieve the desired friction performance. Nevertheless, material properties, such as corrosion resistance, are also crucial performance criteria. This study illuminates the potential for future hybrid tribological characterisations and additional surface treatments to be investigated.

CONCLUSIONS

This paper seeks to elucidate the dry sliding wear characteristics of the Ti13Nb13Zr alloy fabricated through pressure-assisted sintering. The critical findings of the study are presented as follows:

- The CoF coefficient curves, recorded at a sliding distance of 250 m and loads of 10, 15, and 20 N, displayed similar tendencies. The alloy's overall tribological behaviour did not demonstrate a notable variation based on the applied loads. The maximum average CoF value was recorded for the 15 N load.
- A statistical analysis of the CoF values recorded over the sliding distance was conducted. The histogram graphs indicated that the CoF values of the 15 N load exhibited a wide distribution. The standard deviation and other statistical data revealed that the CoF values of the 20 N load were more effective along the sliding distance.
- As the application load intensified, weight reductions likewise intensified. Consequently, the mean CoF values determined by statistical analysis corroborated the sorting results. It was shown that CoF levels and weight loss assessments must be analysed concurrently.
- The analysis of the worn surface was performed utilising scanning electron microscopy (SEM). The mechanisms of abrasion responsible for wear under different loads were described. Furthermore, energy-dispersive spectroscopy (EDS) investigations indicated the production of wear debris and the state of surface oxidation.

The tribological behaviour of the Ti13Nb13Zr alloy, generated via powder metallurgy, was described in the biomedical field, namely in the production of orthopaedic implants. Future research should focus on examining the impacts of various lubricating fluids, corrosive assessments, sintering, and tribological test parameters on the wear behaviour of the alloy.

Data Availability Statement

The author confirm that the data that supports the findings of this study are available within the article. Raw data that support the finding of this study are available from the corresponding author, upon reasonable request.

Conflict of Interest

The author declared no potential conflicts of interest with respect to the research, authorship, and/or publication of this article.

Use of AI for Writing Assistance

Not declared.

Ethics

There are no ethical issues with the publication of this manuscript.

REFERENCES

[1] Abakay, E., Armağan, M., Yıldıran Avcu, Y., Guney, M., Yousif, B. F., & Avcu, E. (2024). Advances in improving tribological performance of titanium alloys and titanium matrix composites for biomedical applications: a critical review. *Frontiers in Materials*, *11*, Article1452288. [CrossRef]

[2] Avcu, Y. Y., Iakovakis, E., Guney, M., Çalım, E., Özkılınç, A., Abakay, E., ... Avcu, E. (2023). Surface and Tribological Properties of Powder Metallurgical Cp-Ti Titanium Alloy Modified by Shot Peening. *Coatings, 13*(1), Article 89. [CrossRef]

[3] Avcu, E., Abakay, E., Yıldıran Avcu, Y., Çalım, E., Gökalp, İ., Iakovakis, E., ... Guney, M. (2023). Corrosion Behavior of Shot-Peened Ti6Al4V Alloy Produced via Pressure-Assisted Sintering. *Coatings, 13*(12), Article 2036. [CrossRef]

[4] Avcu, E., Fidan, S., Yıldıran, Y., & Sınmazçelik, T. (2013). Solid particle erosion behaviour of Ti6Al4V alloy. *Tribology - Materials, Surfaces & Interfaces, 7*(4), 201–210. [CrossRef]

[5] Avcu, E., Yıldıran Avcu, Y., Baştan, F. E., Rehman, M. A. U., Üstel, F., & Boccaccini, A. R. (2018). Tailoring the surface characteristics of electrophoretically deposited chitosan-based bioactive glass composite coatings on titanium implants via grit blasting. *Progress in Organic Coatings, 123*, 362–373. [CrossRef]

[6] Yildiran Avcu, Y., Yetik, O., Guney, M., Iakovakis, E., Sinmazcelik, T., & Avcu, E. (2020). Surface, subsurface and tribological properties of Ti6Al4V alloy shot peened under different parameters. *Materials (Basel), 13*(19), Article 4363. [CrossRef]

[7] Khanlou, H. M. (2012). FE-SEM and EDX characterization of sand blasted and sulfuric acid etched of novel biomaterial (Ti13Nb13Zr). *Australian Journal of Basic and Applied Sciences, 6*(6), 125–131.

[8] Bigi, A., Nicoli-Aldini, N., Bracci, B., Zavan, B., Boanini, E., Sbaiz, F., ... Cortivo, R. (2007). In vitro culture of mesenchymal cells onto nanocrystalline hydroxyapatite-coated Ti13Nb13Zr alloy. *J Biomed Mater Res A, 82*(1), 213–221. [CrossRef]

[9] Golvano, I., Garcia, I., Conde, A., Tato, W., & Aginagalde, A. (2015). Influence of fluoride content and pH on corrosion and tribocorrosion behaviour of Ti13Nb13Zr alloy in oral environment. *Journal of the Mechanical Behavior of Biomedical Materials, 49*, 186–196. [CrossRef]

[10] Suresh, K. S., Gurao, N. P., Singh D, S., Suwas, S., Chattopadhyay, K., Zherebtsov, S. V., & Salishchev, G. A. (2013). Effect of equal channel angular pressing on grain refinement and texture evolution in a biomedical alloy Ti13Nb13Zr. *Materials Characterization, 82*, 73–85. [CrossRef]

[11] Neto, M. Q., & Rainforth, W. M. (2020). Effect of potential and microstructure on the tribocorrosion behaviour of beta and near beta Ti alloys I. *Biotribology, 24*, Article 100141. [CrossRef]

[12] Bansal, P., Singh, G., & Sidhu, H. S. (2021a). Improvement of surface properties and corrosion resistance of Ti13Nb13Zr titanium alloy by plasma-sprayed HA/ZnO coatings for biomedical applications. *Materials Chemistry and Physics, 257*, Article 123738. [CrossRef]

[13] Bansal, P., Singh, G., & Sidhu, H. S. (2021b). Plasma-Sprayed HA/Sr reinforced coating for improved corrosion resistance and surface properties of Ti13Nb13Zr titanium alloy for biomedical implants. *Journal of Materials Research, 36*(2), 431–442. [CrossRef]

[14] Rogala-Wielgus, D., Majkowska-Marzec, B., Zielinski, A., Bartmanski, M., & Bartosewicz, B. (2021). Mechanical behavior of bi-layer and dispersion coatings composed of several nanostructures on Ti13Nb13Zr alloy. *Materials (Basel), 14*(11), Article 2905. [CrossRef]

[15] Bulutsuz, A., Chrominski, W., Lewandowska, M., & Ozaltin, K. (2018). Investigation of different severe plastic deformation methods effect on Ti13Nb13Zr. *Materials Science and Technology*, 664–669. [CrossRef]

[16] Pérez, D. A. G., Jorge Junior, A. M., Roche, V., Lepretre, J.-C., Afonso, C. R. M., Travessa, D. N., ... Botta, W. J. (2020). Severe plastic deformation and different surface treatments on the biocompatible Ti13Nb13Zr and Ti35Nb7Zr5Ta alloys: Microstructural and phase evolutions, mechanical properties, and bioactivity analysis. *Journal of Alloys and Compounds, 812*, Article 152116. [CrossRef]

[17] Dąbrowski, R., & Sołek, K. (2023). Formation of microstructure and mechanical properties of Ti13Nb13Zr medical titanium alloy. *Engineering Science and Technology, an International Journal, 47*, Article 101547. [CrossRef]

[18] Jażdżewska, M., Majkowska-Marzec, B., Ostrowski, R., & Olive, J.-M. (2023). Influence of Surface Laser Treatment on Mechanical Properties and Residual Stresses of Titanium and its Alloys. *Advances in Science and Technology Research Journal, 17*(6), 27–38. [CrossRef]

[19] Jazdzewska, M., Majkowska-Marzec, M., Zielinski, A., Ostrowski, R., Fraczek, A., Karwowska, G., & Olive, J. M. (2023). Mechanical properties and wear susceptibility determined by nanoindentation technique of Ti13Nb13Zr titanium alloy after "direct laser writing". *Materials (Basel), 16*(13), Article 4834. [CrossRef]

[20] Majkowska-Marzec, B., Teczar, P., Bartmanski, M., Bartosewicz, B., & Jankiewicz, B. J. (2020). Mechanical and Corrosion Properties of Laser Surface-Treated Ti13Nb13Zr Alloy with MWCNTs Coatings. *Materials (Basel), 13*(18), Article 3991. [CrossRef]

[21] Pawlowski, L., Mania, S., Banach-Kopec, A., Bartmanski, M., Ronowska, A., Jurak, K., ... Zielinski, A. (2023). Osteoblast and bacterial cell response on RGD peptide-functionalized chitosan coatings electrophoretically deposited from different suspensions on Ti13Nb13Zr alloy. *Journal of Biomedical Materials Research Part B: Applied Biomaterials, 111*(10), 1800–1812. [CrossRef]

[22] Abbas, S. M., Takhakh, A. M., Chiad, J. S., Mohammed, M. A., & Husain, M. A. (2024). Finite-element analysis and ground reaction force of transfemoral osseointegrated prostheses. *Library Progress International, 44*(2), 406–418.

[23] Uchoa, J. D., Santana, M., Rodrigues, M. V. G., Jorge, A. J. r., Pessoa, R. S., Viana, B. C., ... & Lobo, A. O. (2023). Optimizing surface properties of Ti13Nb13Zr alloy substrate for biomedical applications through modification with nano-alumina obtained by atomic layer deposition and hydroxyapatite coatings. *Surface & Coatings Technology, 468*, Article 129755. [CrossRef]

[24] Sypniewska, J., Szkodo, M., Majkowska-Marzec, B., & Mielewczyk-Gryn, A. (2023). Effect of hybrid modification by ceramic layer formation in MAO process and laser remelting on the structure of titanium bio-alloy Ti13Nb13Zr. *Ceramics International, 49*(11), 16603–16614. [CrossRef]

[25] Jorge, A. M., Roche, V., Pérez, D. A. G., & Valiev, R. Z. (2023). Nanostructuring Ti-alloys by HPT: Phase transformation, mechanical and corrosion properties, and bioactivation. *Materials Transactions, 64*(7), 1306–1316. [CrossRef]

[26] Rościszewska, M., Shimabukuro, M., Ronowska, A., Mielewczyk-Gryń, A., Zieliński, A., & Hanawa, T. (2024). Enhanced bioactivity and mechanical properties of silicon-infused titanium oxide coatings formed by micro-arc oxidation on selective laser

melted Ti13Nb13Zr alloy. *Ceramics International, 50*(21), 43979–43993. [CrossRef]

[27] Aslan, A. K., (2024). Tribological properties of the multilayer thin films deposited on the free-form shaped Ti13Nb13Zr alloy. *Jurnal Tribologi, 42*, 129–145.

[28] Aslan, A. K., & Bahce, E. (2023). Wear and Adhesion Properties of Multilayer Ti/TiN, (/TiC)/ TiCN/ TaN Thin Films Deposited on Ti13Nb13Zr Alloy by Closed Field Unbalanced Magnetron Sputtering. *Acta Metallurgica Slovaca, 29*(4), 192–199. [CrossRef]

[29] Lison, J., Taratuta, A., Paszenda, Z., Dyner, M., & Basiaga, M. (2022). A study on the physicochemical properties of surface modified Ti13Nb13Zr alloy for skeletal implants. *Acta of Bioengineering and Biomechanics, 24*(1), 39–47. [CrossRef]

[30] Piotrowska, K., Granek, A., & Madej, M. (2020). Assessment of mechanical and tribological properties of diamond-like carbon coatings on the Ti13Nb13Zr alloy. *Open Engineering, 10*(1), 536–545. [CrossRef]

[31] Neto, M. Q., & Rainforth, W. M. (2021). Effect of potential and microstructure on the tribocorrosion behaviour of beta and near beta Ti alloys II. *Journal of Bio- and Tribo-Corrosion, 7*(4), Article 141. [CrossRef]

[32] Piotrowska, K., & Madej, M. (2022). Influence of TiO2 coating deposited with the atomic layer deposition ALD technique on the properties of Ti13Nb13Zr titanium alloy. *Metalurgija, 61*(3-4), 665–668.

[33] Piotrowska, K., Madej, M., Kowalczyk, J., & Radon-Kobus, K. (2023). Surface roughness effects on the properties of silicon-doped diamond-like carbon coatings. *Coatings, Vol. 13*(9), Article 1629. [CrossRef]

[34] Seramak, T., Zielinski, A., Serbinski, W., & Zasinska, K. (2019). Powder metallurgy of the porous Ti-13Nb-13Zr alloy of different powder grain size. *Materials and Manufacturing Processes, 34*(8), 915–920. [CrossRef]

[35] Avcu, E. (2017). The influences of ECAP on the dry sliding wear behaviour of AA7075 aluminium alloy. *Tribology International, 110*, 173–184. [CrossRef]

[36] Gökalp, İ., Kıraç, M., Avcu, E., & Yamanoğlu, R. (2023). Dental uygulamalarda kullanılan CoCr alaşımının tribolojik özeliklerinin incelenmesi. In S. K. Ferit Kargın (Ed.), *Doğa ve Mühendislik Bilimlerinde Güncel Tartışmalar 12* (pp. 114–123). Bidge Yayıncılık.

[37] Yıldıran Avcu, Y., Yetik, O., Koçoğlu, H., Avcu, E., & Sınmazçelik, T. (2018). Dry Sliding Wear Behaviour of Shot Peened TI6AL4V Alloys at Different Peening Times. *Acta Physica Polonica A, 134*(1), 349–353. [CrossRef]

[38] Yamanoglu, R., Bahador, A., & Kondoh, K. (2021). Effect of Mo Addition on the Mechanical and Wear Behavior of Plasma Rotating Electrode Process Atomized Ti6Al4V Alloy. *Journal of Materials Engineering and Performance, 30*(5), 3203–3212. [CrossRef]

[39] Yamanoglu, R. (2021). Network distribution of molybdenum among pure titanium powders for enhanced wear properties. *Metal Powder Report, 76*(1), 32–39. [CrossRef]

[40] Ahmad, K., Batool, S. A., Farooq, M. T., Minhas, B., Manzur, J., Yasir, M., ... Ur Rehman, M. A. (2023). Corrosion, surface, and tribological behavior of electrophoretically deposited polyether ether ketone coatings on 316L stainless steel for orthopedic applications. *Journal of the Mechanical Behavior of Biomedical Materials, 148*, Article 106188. [CrossRef]

[41] Iakovakis, E., Avcu, E., Roy, M. J., Gee, M., & Matthews, A. (2021). Dry sliding wear behaviour of additive manufactured CrC-rich WC-Co cemented carbides. *Wear, 486-487*, Article 204127.

[42] Yamanoglu, R., Karakulak, E., Zeren, M., & Koç, F. G. (2013). Effect of nickel on microstructure and wear behaviour of pure aluminium against steel and alumina counterfaces. *International Journal of Cast Metals Research, 26*(5), 289–295. [CrossRef]

[43] Yamanoğlu, R., Karakulak, E., Zeren, A., & Zeren, M. (2013). Effect of heat treatment on the tribological properties of Al–Cu–Mg/nanoSiC composites. *Materials & Design, 49*, 820–825. [CrossRef]

[44] Laraba, S. R., Rezzoug, A., Avcu, E., Luo, W., Halimi, R., Wei, J., & Li, Y. (2023). Enhancing the tribological performance of PLA-based biocomposites reinforced with graphene oxide. *Journal of the Mechanical Behavior of Biomedical Materials, 148*, Article 106224. [CrossRef]

[45] Mameri, A., Daoud, I., Rezzoug, A., Azem, S., & Yamanoglu, R. (2022). Tribological properties of in situ oxide reinforced nickel matrix composites produced by pressure-assisted sintering. *The International Journal of Advanced Manufacturing Technology, 120*(5-6), 3731–3740. [CrossRef]

[46] Mameri, A., Daoud, I., Rezzoug, A., Boukantar, A.-R., Miroud, D., Yamanoglu, R., & Ortiz, A. L. (2024). Effect of Ni aids on the unlubricated tribological behaviour of WC cemented carbides fabricated by pressureless infiltration of Cu alloy binder. *Ceramics International*, In Press. doi: 10.1016/j.ceramint.2024.11.287 [CrossRef]